Inorganic Chemistry

Article

pubs.acs.org/IC

Copper(I) and Silver(I) 2-Methylimidazolates: Extended Isomerism, Isomerization, and Host–Guest Properties

Yu Wang, Chun-Ting He, Yi-Jiang Liu, Tian-Qi Zhao, Xiao-Min Lu, Wei-Xiong Zhang, Jie-Peng Zhang,* and Xiao-Ming Chen

MOE Key Laboratory of Bioinorganic and Synthetic Chemistry, KLGHEI of Environment and Energy Chemistry, School of Chemistry and Chemical Engineering, Sun Yat-Sen University, Guangzhou 510275, China

Supporting Information

ABSTRACT: Syntheses, structures, and properties of univalent coinage metal 2-methylimidazolate supramolecular isomers [M(mim)] (**1**, M = Cu; **2**, M = Ag) were investigated in detail. In addition to the known isomers, namely, zigzag chains [Cu(mim)] (**1a**) and [Ag(mim)] (**2a**), molecular octagon $[Cu_8(mim)_8]\cdot C_6H_6$ (**1b**), decagon $[Cu_{10}(mim)_{10}]\cdot C_8H_{10}$ (**1c**), helical chain $[Ag_4(mim)_4]\cdot C_6H_6$ (**2b**), and S-shaped chain $[Ag_4(mim)_4]\cdot C_8H_{10}$ (**2c**), two new structures including a polyrotaxane $[Cu_{10}(mim)_{10}]\cdot[Cu(mim)]$ (**1d**, *C*2/*m*, *a* = 14.452(4) Å, *b* = 27.712(7) Å, *c* = 11.427(3) Å, *β* = 125.899(4)°, *V* = 3707(2) Å^3) and a new octagon $[Ag_8(mim)_8]\cdot Me_2CO$ (**2d**, *C*2/*c*, *a* = 21.852(3) Å, *b* = 12.101(2) Å, *c* = 20.907(3) Å, *β* = 90.875(2)°, *V* = 5528(2) Å^3) were discovered. The potential porous properties of guest-containing [M(mim)] isomers were studied by thermogravimetry, X-ray powder diffraction, vacuum thermal desorption, and CO_2 sorption experiments. The isomers show distinctly different guest removal behaviors depending on their pore structures. By heating, the guest-containing isomers, **1b**–**1c** and **2b**–**2d**, undergo irreversible, two-step, crystal-to-crystal structural transformations to form the guest-free isomers **1a** or **2a**, respectively. Except **1b**, other guest-containing isomers can retain their porous structures after removal of the template molecules, which were confirmed by CO_2 sorption experiments.

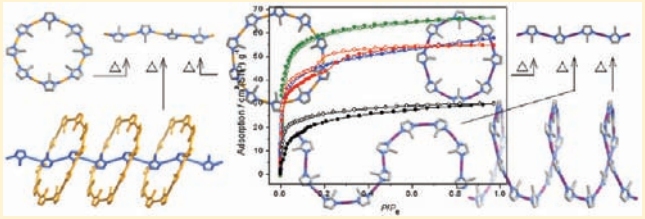

INTRODUCTION

Coordination polymers have attracted a great deal of academic and commercial interest due to their fascinating structures and potential applications.[1] Controlling the structures and properties of coordination polymers is a long-standing challenge.[2] Supramolecular isomerism,[3] as an interesting phenomenon in supramolecular and coordination chemistry,[4] plays an important role in understanding the self-assembly and structure–property relationship of coordination polymers.[5] Guest-induced supramolecular isomers have been well documented, which can be obtained by rational introduction of different template molecules. Strictly speaking, isomeric frameworks depending on inclusion of different guest molecules are not genuine supramolecular isomers, because the crystals have different chemical compositions. However, if the template molecules can be removed, these crystals become genuine supramolecular isomers with different porous structures.[5a] Nevertheless, the potential porosity of guest-induced supramolecular isomers has received little attention.[6]

Metal azolate frameworks (MAFs)[7] have been demonstrated as a simple and effective metal–ligand system for the construction of supramolecular isomers.[5a] Univalent coinage metal imidazolates are straightforward for simple chain-like polymeric structures, because the exobidentate ligand enforces univalent coinage metal to be linear two-coordinated. Further, the moderate bridging angle of imidazolate (ca.135–140°) renders not only ordinary zigzag chains but also highly curved helical chains, large polygons, and other unusual superstructures. Among a variety of imidazolate derivatives, 2-methylimidazolate showed the most abundant structure diversity and only one case of template-induced isomerism, which may be due to the fact that methyl group has a suitable size to interact with guest and avoid too much steric hindrance. We have isolated a series of supramolecular isomers of Cu(I)/Ag(I) 2-methylimidazolates (Figure 1). For example, close-packing zigzag chains of [Cu(mim)] (**1a**) and [Ag(mim)] (**2a**) were obtained without template. Molecular octagon $[Cu_8(mim)_8]\cdot C_6H_6$ (**1b**) and 8_1 helix $[Ag_4(mim)_4]\cdot C_6H_6$ (**2b**) were isolated using benzene as template, while larger template *p*-xylene gave molecular decagon $[Cu_{10}(mim)_{10}]\cdot C_8H_{10}$ (**1c**) and S-shaped chain $[Ag_4(mim)_4]\cdot C_8H_{10}$ (**2c**).[8] It is worth noting that, although Cu(I) and Ag(I) possess the same coordination mode, the structures of [Cu(mim)] and [Ag(mim)] polymers are very different. For instance, a Ag(I)-based molecular polygon has not been observed previously, which has been attributed to the differences of ionic radius and metallophilicity that change the sizes and packing fashions of the polygons.[5a] Certainly, such a reasonable, hypothetic isomer may be realized by more extensive synthetic studies. Also, considering that current studies on porous coordination polymers (PCPs) are mostly

Received: January 13, 2012
Published: April 2, 2012

   dx.doi.org/10.1021/ic300083k | *Inorg. Chem.* 2012, 51, 4772–4778

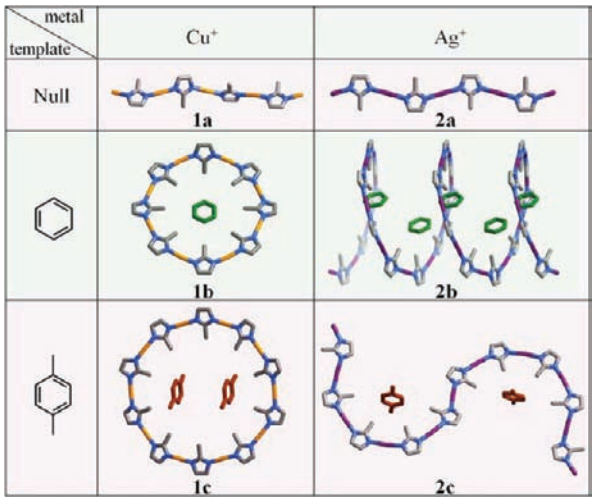

Figure 1. Known supramolecular isomers of **1** and **2**.

focused on three-dimensional (3D) or two-dimensional (2D) coordination frameworks, these template-induced isomers, [M(mim)]·guest, may serve as unique 0D and 1D porous frameworks.[9]

As an extension of our previous crystal engineering study on univalent coinage metal 2-methylimidazolates, here,we report a detailed study on the syntheses, structures, and properties of this unique coordination polymer system. Besides the optimized synthetic method and discovery of new supramolecular isomers, thermal stabilities, structural dynamic behaviors, and porous properties of the guest containing isomers were also investigated.

EXPERIMENTAL SECTION

Materials and General Methods. All solvents and starting materials were purchased commercially and used as received. Elemental analyses (EA) were performed by a Perkin-Elmer 240 elemental analyzer (C, H, N). Thermogravimetric (TGA) analyses were performed at a rate of 3 °C/min under N_2 using a NETZSCH TG 209 system. Vacuum thermal desorption (VTD) was performed at a rate of 3 °C/min using the degas port of a Micromeritics ASAP 2020 M instrument equipped with a turbo molecular pump and a μmHg pressure gauge. Powder X-ray diffraction (PXRD) data were recorded on a Bruker D8 ADVANCE X-ray powder diffractometer (Cu Kα). In variable-temperature powder X-ray diffraction (VTPXRD) measurements, the diffraction patterns for different temperatures were recorded after the sample had stayed at the respective temperature for 30 min. Differential scanning calorimetry (DSC) was performed under N_2 using a Netzsch DSC 204 system under N_2. CO_2 sorption measurements were performed using a Belsorp-Max automatic volumetric adsorption apparatus.

Syntheses. *Cu(I) 2-Methylimidazolate Isomers.* A mixture of $Cu(NO_3)_2{\cdot}3H_2O$ (0.242 g, 1.0 mmol), Hmim (0.081 g,1.0 mmol), and aqueous ammonia (25%, 5 mL), as well as an appropriate template if necessary, was stirred for 15 min in air, then transferred and sealed in a 10 mL Teflon-lined vessel, which was heated in an oven to 160 °C for 80 h, and then cooled to room temperature at a rate of 5 °C h^{-1}. The resulting crystals were filtered, washed by ethanol, and dried under N_2. The phase purity of each sample was verified by PXRD.

*[Cu(mim)] (**1a**).* No template was used (yield ca. 10%). EA calcd (%) for $C_4H_5CuN_2$: C 33.22, H 3.48, N 19.37; found: C 33.14, H 3.68, N 19.04.

*[$Cu_8(mim)_8$]·C_6H_6 (**1b**).* Benzene (2 mL) was used as the template (yield ca. 25%). EA calcd (%) for $C_{38}H_{46}Cu_8N_{16}$: C 36.95, H 3.75, N 18.14; found: C 36.61, H 3.96, N 17.93.

*[$Cu_{10}(mim)_{10}$]·2C_8H_{10} (**1c**).* *p*-Xylene (2 mL) was used as the template (yield ca. 45%). EA calcd (%) for $C_{56}H_{70}Cu_{10}N_{20}$: C 40.55, H 4.25, N 16.89; found: C 40.95, H 4.39, N 16.50. A few crystals of $[Cu_{10}(mim)_{10}]{\cdot}[Cu(mim)]$ (**1d**), which did not crack during heating and vacuum treatments, could be found occasionally.

Phase-pure microcrystalline powder can be also prepared by pouring a solution of $[Cu(NH_3)_2]OH$ (1.0 mmol) in aqueous ammonia/methanol (10/10 mL) into a solution of Hmim (1.0 mmol, 0.081 g) in methanol (20 mL) or methanal/template (10/10 mL) with rapid stirring constantly, followed by filtration, wash, and drying. The whole process must be carried out in N_2 atmosphere, but the final products easily turn green in air.

Ag(I) 2-Methylimidazolate Isomers. A solution of Ag_2O (1 mmol, 0.120 g) in aqueous ammonia/ethanol (5/5 mL) was poured into a solution of Hmim (1 mmol, 0.081 g) in methanol (10 mL) or methanal/template (5/5 mL) with rapid stirring constantly. White precipitate appeared quickly, and the slurry was stirred for 15 min. After then, the white powder was filtered, washed by ethanol, and dried in air. The phase purity was verified by PXRD.

*[Ag(mim)] (**2a**).* No template was used (yield ca. 72%). EA calcd (%) for $C_4H_5AgN_2$: C 25.42, H 2.67, N 14.82; found: C 25.59, H 3.03, N 14.78.

*[$Ag_4(mim)_4$]·C_6H_6 (**2b**).* Benzene (5 mL) was used as the template (yield 74%). EA calcd (%) for $[Ag_4(mim)_4]{\cdot}0.6C_6H_6$ ($C_{19.6}H_{23.6}Ag_4N_8$): C 29.33, H 2.96, N 13.96; found: C 29.25, H 3.35, N 13.59. The chemical formula was also supported by TG results, which indicated that the bulk sample was not fully saturated by benzene, or the guest molecules were removed partially after the washing and drying procedures.

*[$Ag_4(mim)_4$]·C_8H_{10} (**2c**).* *p*-Xylene (5 mL) was used as the template (yield 77%). EA calcd (%) for $C_{24}H_{30}Ag_4N_8$: C 33.44, H 3.51, N 13.00; found: C 33.09, H 3.68, N 13.34.

*[$Ag_8(mim)_8$]·0.5Me_2CO·0.5H_2O (**2d**).* Acetone (5 mL) was used as the template (yield 79%). EA calcd (%) for $C_{33.5}H_{44}Ag_8N_{16}O$: C 25.96, H 2.86, N 14.46; for guest-free $[Ag_8(mim)_8]$ ($C_{32}H_{40}Ag_8N_{16}$): C 25.42, H 2.67, N 14.82; found: C 25.92, H 3.05, N 14.73. Single crystals of **2d** were obtained by layering a solution of Hmim (0.1 mmol, 0.008 g) in acetone (2 mL) on a solution of Ag_2O (0.1 mmol, 0.012 g) in aqueous ammonia (25%, 2.0 mL).

X-ray Crystallography. Single-crystal X-ray diffraction data for **1d** and **2d** were collected on a Bruker Apex CCD area-detector diffractometer with Mo Kα monochromatic radiation. The structures were solved by the direct method and refined by the full-matrix least-squares method on F^2 using the SHELXTL software package. All hydrogen atoms were placed geometrically, and anisotropic thermal parameters were used to refine all nonhydrogen atoms. The crystal data and structure refinement results are listed in Table 1.

Density Functional Theory (DFT) Studies. Full geometry optimization was carried out for the model molecules based on the crystal data with the Perdew, Burke, and Ernzerhof (PBEPBE) functional for both exchange and correlation,[10] which was usually thought to give good results for weak intermolecular interactions. Considering both the calculation cost and the accuracy, we used the effective core potential (ECP) and Stuttgart-Dresden ECP plus DZ (SDD) basis sets for transition metal elements (Ag or Cu) and 6-31G (d) for the rest atoms in the geometry optimization. Considering that the local spin density approximation (LSDA) usually overestimates the binding energy, while the generalized gradient approximation (GGA) significantly underestimates, both the LSDA and PBEPBE (one of the GGA functional) method were investigated. Simultaneously, the 6-311G (d, p) basis set was used for C, N, O, and H, and the SDD basis set with ECP was used for transition metal elements with correcting basis set superposition error effects (BSSE). The binding energy ΔE was calculated by:

$$\Delta E = E_{\text{octagon}\cdot n\text{template}} - E_{\text{octagon}} - nE_{\text{template}} + E_{\text{BSSE}}$$

Where n is the number of template molecules, $E_{\text{octagon}\bullet n\text{template}}$, E_{octagon}, E_{template}, and E_{BSSE} are the energies of the complex consisting of an octagon and n template molecules, the single molecular octagon, the

dx.doi.org/10.1021/ic300083k | Inorg. Chem. 2012, 51, 4772−4778

Table 1. Crystallographic Data and Structure Refinement Details[a]

	1	2
formula	$C_{44}H_{63}Cu_{11}N_{22}O_4$	$C_{36.5}H_{51}Ag_8N_{16}O_{2.5}$
FW	1663.1	1616.89
T/K	113(2)	123(2)
space group	$C2/m$	$C2/c$
a/Å	14.452(4)	21.852(3)
b/Å	27.712(7)	12.101(2)
c/Å	11.427(3)	20.907(3)
β/deg	125.899(4)	90.875(2)
V/Å^3	3707(2)	5528(2)
Z	2	4
D_c/g cm^{-3}	1.490	1.943
μ/mm^{-1}	3.134	2.817
R_1 ($I > 2\sigma$)	0.0776	0.0614
wR_2 (all data)	0.2192	0.1712
GOF	1.087	1.071

[a] $R_1 = \sum||F_o| - |F_c||/\sum|F_o|$, $wR_2 = [\sum w(F_o^2 - F_c^2)^2/\sum w(F_o^2)^2]^{1/2}$.

single template molecule, and the BSSE correction, respectively. All calculations were carried out using Gaussian 03 package.

RESULTS AND DISCUSSION

Syntheses. Having very low solubility, metal imidazolate frameworks easily precipitate as microcrystalline powders. The growth of single crystals for X-ray structure analysis often requires using a solvothermal or liquid diffusion method.[5a,7] In our preliminary studies, single crystals of the [Cu(mim)] (**1a**), $[Cu_8(mim)_8]\cdot C_6H_6$ (**1b**), and $[Cu_{10}(mim)_{10}]\cdot C_8H_{10}$ (**1c**) were discovered by solvothermal reactions,[8a] while [Ag(mim)] (**2a**), $[Ag_4(mim)_4]\cdot C_6H_6$ (**2b**), and $[Ag_4(mim)_4]\cdot C_8H_{10}$ (**2c**) were furnished by liquid diffusion reactions.[8b]

In order to optimize the synthesis of these compounds and search for new isomers, we tried different reaction methods and conditions. Rapid mixing an aqueous ammonia solution of metal oxide/hydroxide with a solution of ligands has been demonstrated to be efficient for producing a pure microcrystalline sample for several MAF systems.[11] This method can be applied for not only rapid syntheses of known isomers but also discovery of new isomers of Cu(I) and Ag(I) 2-methylimidazolates. Nevertheless, the rapid solution mixing method for Cu(I) complexes requires inert atmosphere protection, and the powder of Cu(I) 2-methylimidazolates obtained by this method tends to be oxidized in air, probably due to their small particle sizes. Therefore, the more convenient solvothermal method, despite its long reaction time and relatively low yield, was used for preparation of the Cu(I) 2-methylimidazolate isomers, for which the large single crystals can be handled in the air.

Although liquid diffusion can produce high-quality single crystals of Ag(I) 2-methylimidazolate isomers, it also has many drawbacks such as long reaction time, low yield, low purity, and/or low repeatability. The crystals of guest-containing isomers generally grow at the template buffering layer, while the guest-free isomer **1a** always appears at other places simultaneously. Ag(I) ions are relatively stable in air but can be easily reduced at high temperatures so that the solvothermal method is not suitable for Ag(I) 2-methylimidazolates. Therefore, the rapid solution mixing method is suitable for synthesizing the Ag(I) 2-methylimidazolate isomers. More importantly, using acetone as a solvent, a new structure was obtained, as evident by PXRD characterization. Fortunately, single crystals of the new phase, i.e., the octagon $[Ag_8(mim)_8]\cdot Me_2CO$ (**2d**), were latterly obtained by the liquid diffusion reaction, which enable structure determination in spite of poor reproducibility and low yield. It is worth noting that the mixing speed of metal ions and ligands has great impact on the product purity. Only quickly pouring the aqueous ammonia of Ag_2O into the methanol solution of Hmim can generate the guest-containing phases **2b**, **2c**, and **2d** as pure phases. Otherwise, the products always contain **2a** as an impurity, indicating that the zigzag chain structure is the thermodynamically favored phase, and the guest-containing structures are kinetic favored ones (Figure S1, Supporting Information).

Structures. As expected, the univalent coinage metal imidazolate frameworks are all constructed by linear coordinated metal ions and exobidentate mim$^-$ ligands. Depending on the related orientation of the adjacent ligands, these structurally simple coordination polymers can form different superstructures, including zigzag chains, helical chains, and polygons. Among various reported imidazolate derivatives, mim$^-$ is the most special one because its superstructure can be controlled by appropriate templates. Without adding guest molecules, adjacent mim$^-$ ligands adopt approximately trans-configuration, giving rise to close-packing zigzag chains **1a** and **2a**.

Using aromatic templates with different sizes, Cu(I) 2-methylimidazolate crystallize as molecular octagons **1b** and decagons **1c**. If the guests were removed from **1b** and **1c**, the void would be 20.5% and 39.7%, respectively,[12] suggesting potential porosity. However, because of the staggered stacking of octagons, the cavities inside the octagons (6.5 × 9.5 × 7.5 Å^3) are not interconnected (aperture diameter 3.4 Å) to each other in **1b**. Although the decagons stack in a similar fashion, the larger inner cavities (8.6 × 10.3 × 11.5 Å^3) are connected large apertures (6.1 × 8.6 Å^2) to form 1D channels in **1c** (Figure 2).

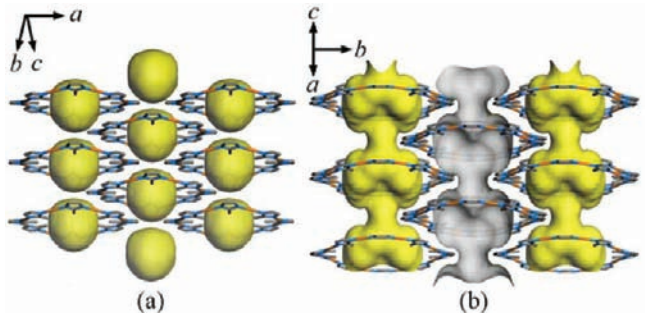

Figure 2. Perspective views of the framework and pore (shown as Connolly surfaces with probe diameter 2.5 Å) structures of (a) **1b** and (b) **1c**.

While single crystals of **1c** tend to crack during thermal and/or vacuum treatments, a few specimens remain intact, which were identified as a polyrotaxane-like structure $[Cu_{10}(mim)_{10}]\cdot[Cu(mim)]$ (**1d**) by X-ray single-crystal diffraction study. Having very similar cell parameters and the same space group with **1c**, **1d** also contains the $[Cu_{10}(mim)_{10}]$ decagons, but its cavities are occupied by Cu(I) ions and mim$^-$ ligands rather than the xylene molecules. Interestingly, the extra Cu(I) ions and mim$^-$ ligands connect each other into simple zigzag chains penetrating through multiple decagons, which form a rare polyrotaxane-like structure (Figure 3). Masciocchi et al. have reported a cocrystal structure of chain and ring

dx.doi.org/10.1021/ic300083k | Inorg. Chem. 2012, 51, 4772−4778

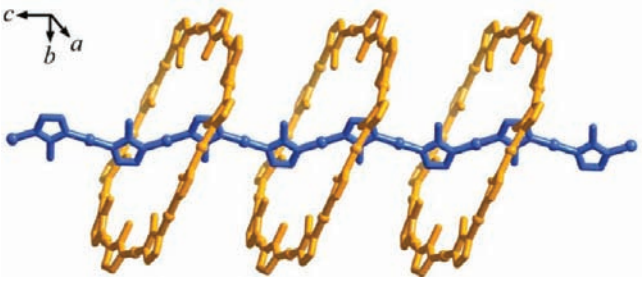

Figure 3. Perspective view of the polyrotaxane-like structure of **1d**.

isomers for [Cu(pymo)] (Hpymo = 2-hydroxypyrimidine), in which the small $[Cu_6(pymo)_6]$ hexagons are not penetrated by the steric hindered helical chains.[13]

Being different with Cu(I) 2-methylimidazolate, Ag(I) 2-methylimidazolate containing aromatic templates are 8_1 helix chains and S-shaped chains instead of polygons. The potential voids in **2b** and **2c** would be 22.5 and 25.6%, respectively, when the template molecules are omitted. Packing of the highly curved chains leads to S-shaped channels, with widest and narrowest cross section sizes of ca. 7.1 × 4.3 Å^2 and 7.6 × 3.8 Å^2 for **2b**, and 6.7 × 3.9 Å^2 and 7.7 × 3.2 Å^2 for **2c**, respectively (Figure 4).

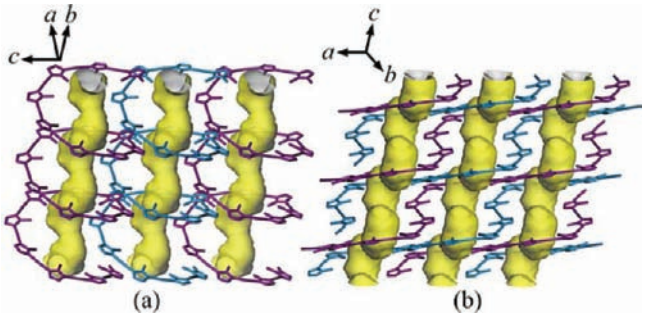

Figure 4. Perspective views of the framework and pore (shown as Connolly surfaces with probe diameter 2.5 Å) structures of (a) **2b** and (b) **2c**.

Crystal structure analysis showed that **2d** contains four independent linear two-coordinated Ag(I) ions and four exobidentate mim$^-$ ligands (Ag–N 2.056(9)–2.099(9) Å, N–Ag–N 170.6(4)–177.0(4)°), as well as disordered acetone and water guest molecules. The adjacent mim$^-$ ligands are oriented in a *cis*-fashion (the dihedral angle, DA, between adjacent im rings is 8.6–29.3°), giving rise to a semicircular-shaped $Ag_4(mim)_4$ fragment. Two of such fragments join (DA 24.1°) to generate a centrosymmetric, neutral, flattened elliptical octagon (Figure 5a). The inner cavity of **2d** has a size of (7.0 × 10.0 Å^2), which is slightly larger than that of the Cu(I) analog **1b** (6.5 × 9.5 Å^2). Comparison of the cavity sizes with the molecular sizes of benzene (6.6 × 7.3 Å^2), cyclohexane (6.6 × 7.2 Å^3), and *p*-xylene (6.6 × 9.1 Å^3) indicates that the guests are suitable for **1b** but smaller for **2d** as template (Figure 5b). Similar to other univalent coinage metal imidazolates, $[Ag_8(mim)_8]$ also stack by metallophilic interactions (Ag1···Ag3 2.9996(12) Å, Ag1···Ag4 2.9870(13) Å, Ag2···Ag4 3.0530(12) Å) to form high-dimensional structure (Figure 5c). There are 1D curved channels (void = 26.7%) with the narrowest and widest diameter ca. 4.3 Å and 10.0 Å, respectively, running along the *c*-axis. (Figure 5d).

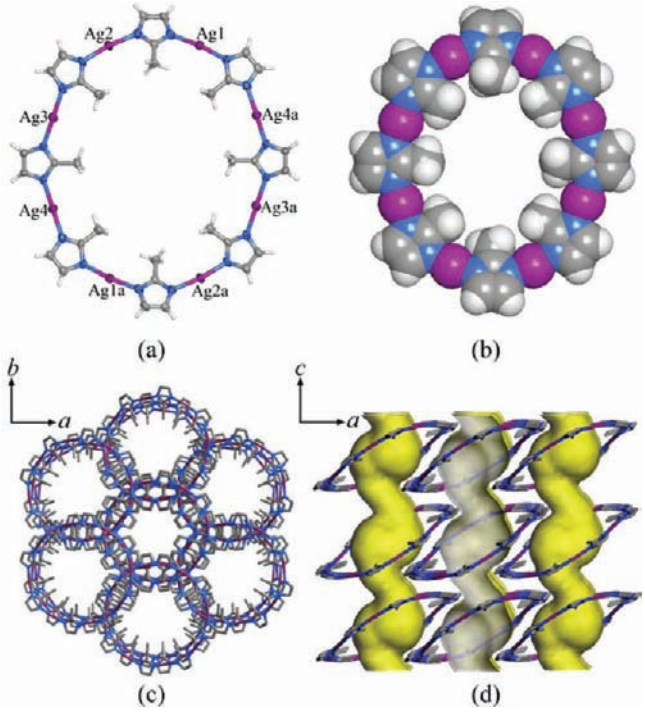

Figure 5. Perspective views of the octagonal molecular structure in (a) ball-and-stick (thermal ellipsoid drawn at 50% probability. Symmetry code: a = 1 − *x*, −*y*, 1 − *z*) and (b) space-filling mode, and (c) packing of octagons and (d) pore structure (shown as Connolly surfaces with probe diameter 2.5 Å) of **2d**.

Theoretical Study. To further understand the template effect involved in the syntheses of these compounds, we used density functional theory (DFT) to calculate the binding energy (ΔE) of the $[Cu_8(mim)_8]/[Ag_8(mim)_8]$ octagons with different guest molecules (observed in the crystal structures or hypothetic) (Figure S2 and Tables S1–S8, Supporting Information). As shown in Table 2, both benzene and toluene

Table 2. Calculated Binding Energies of $[M_8(mim)_8]$ Octagons for Different Guests

host + guest	PBEPBE (kJ/mol)	LSDA (kJ/mol)
$[Ag_8(mim)_8]$ + benzene	−1.78	−8.57
$[Cu_8(mim)_8]$ + benzene	−7.28	−18.43
$[Ag_8(mim)_8]$ + toluene	−2.40	−13.28
$[Cu_8(mim)_8]$ + toluene	−8.49	−23.33
$[Ag_8(mim)_8]$ + 2acetone	−15.06	−25.48
$[Cu_8(mim)_8]$ + 2acetone	−31.32	−67.44

can be inserted into the $[Cu_8(mim)_8]$ and $[Ag_8(mim)_8]$ octagons with attractive interactions (binding energy ΔE < 0). However, the binding energy of $[Cu_8(mim)_8]$ with benzene and toluene are 6–10 kJ·mol^{-1} larger than those for $[Ag_8(mim)_8]$, indicating that the stabilization effects of benzene and toluene for $[Cu_8(mim)_8]$ are stronger than for $[Ag_8(mim)_8]$. The difference can be explained by the relatively large inner cavity of $[Ag_8(mim)_8]$, which has weak confinement effect for benzene and toluene. On the other hand, when a pair of acetone molecules were inserted into the $[Ag_8(mim)_8]$ octagon, the binding energy was much lower than for those containing aromatics, which was consistent with our experimental results. It can be explained that the size of a pair of acetone molecules are suitable for the cavity size of

dx.doi.org/10.1021/ic300083k | *Inorg. Chem.* 2012, 51, 4772–4778

$[Ag_8(mim)_8]$ octagon. Unexpectedly, the binding energy of $[Cu_8(mim)_8]$ octagon with a pair of acetone molecules was the lowest among all calculation results, indicating that a pair of acetone molecules could be also inserted into a smaller pore, illustrating the flexible nature of the supramolecular acetone dimer. This result also suggests that acetone may also promote the formation of $[Cu_8(mim)_8]$ octagons. As predicted, the microcrystalline product obtained by rapid solution mixing reaction of Cu(I) 2-methylimidazolate using acetone as the template displays a PXRD pattern (Figure S1g, Supporting Information) very similar to that of **1b**.

Framework Stability. Similar to other univalent coinage metal azolates, Cu(I) and Ag(I) 2-methylimidazolates also have good chemical stability. Crystal samples of isomers **1a**−**1c** can be handled in air for short time, and its color changes from yellow to light green after 2 days, reflecting the oxidation of Cu(I) ions in air and moisture. However, after 1 month of exposure, the PXRD pattern of the light-green crystals still resembled that of isomers **1a**−**1c**, respectively. For samples of isomers **2a**−**2d**, no color change was evident when powder samples were exposed to ambient light for weeks.

Thermal stability and template removing property of **1b**, **1c**, **2b**, **2c**, and **2d** were estimated by thermogravimetry (TG) and variable-temperature PXRD (VTPXRD) measurements. TG curve of **1b** showed a weight loss 6.36% (cal. 6.32%) between 165 and 240 °C, followed by a plateau to 350 °C. The initial guest removal temperature is much higher than the boiling point of benzene, corresponding well to the unconnected cavities. In contrast, **1c** containing 1D S-shape channel began to lose weight at 60 °C, and all *p*-xylene can be removed below 170 °C (Figure 6).

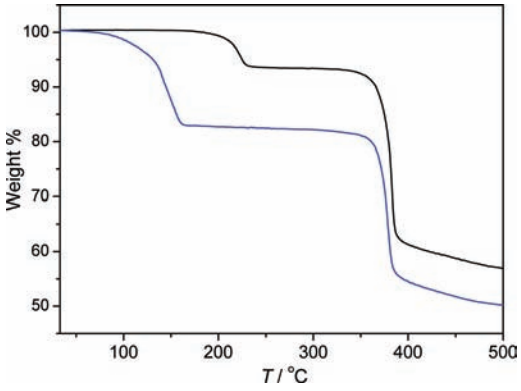

Figure 6. TG curves of **1b** (black) and **1c** (blue).

TG curves of **2b** and **2c** are similar, which lose weight from room temperature to 155 °C, and decompose above 220 °C. It is interesting that the TG curve of **2d** did not show the guest removal process, although its decomposed temperature was similar to those of **2b** and **2c** (Figure 7). This phenomenon can be explained by the large pores of **2d**, which can hardly retain the guest molecules with low boiling point and small size after routine filtration, washing, and drying procedures.

VTPXRD patterns of **1b** showed that the as-synthesized phase can be stable up to 160 °C. New diffraction peaks appeared at 180 °C, which became stronger and stronger below 240 °C. This phenomenon is consistent with the guest removal temperature range in the TG curve. The as-synthesized phase disappeared above 240 °C. At 250 °C, some other new peaks appeared, and the sample completely transformed to another

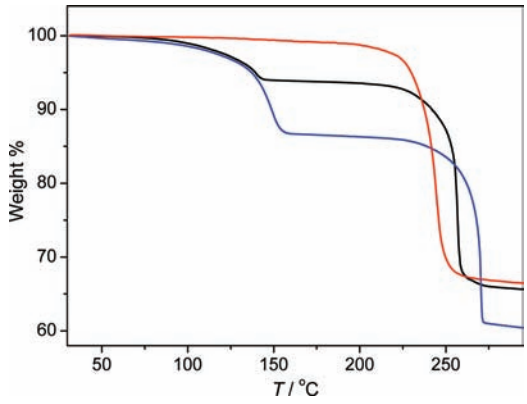

Figure 7. TG curves of **2b** (black), **2c** (blue), and **2d** (red).

phase above 260 °C, corresponding well with the plateau in the TG curve (Figure 8a). Similarly, **1c** also transformed to two new phases at 120 and 250 °C, respectively (Figure 8b).

Interestingly, the diffraction patterns of the first and second new phases of **1b** are very similar to those of the first and second ones of **1c**, respectively. Moreover, the diffraction patterns of the second new phases were very similar to that of **1a**, indicating that both **1b** and **1c** finally transformed to the

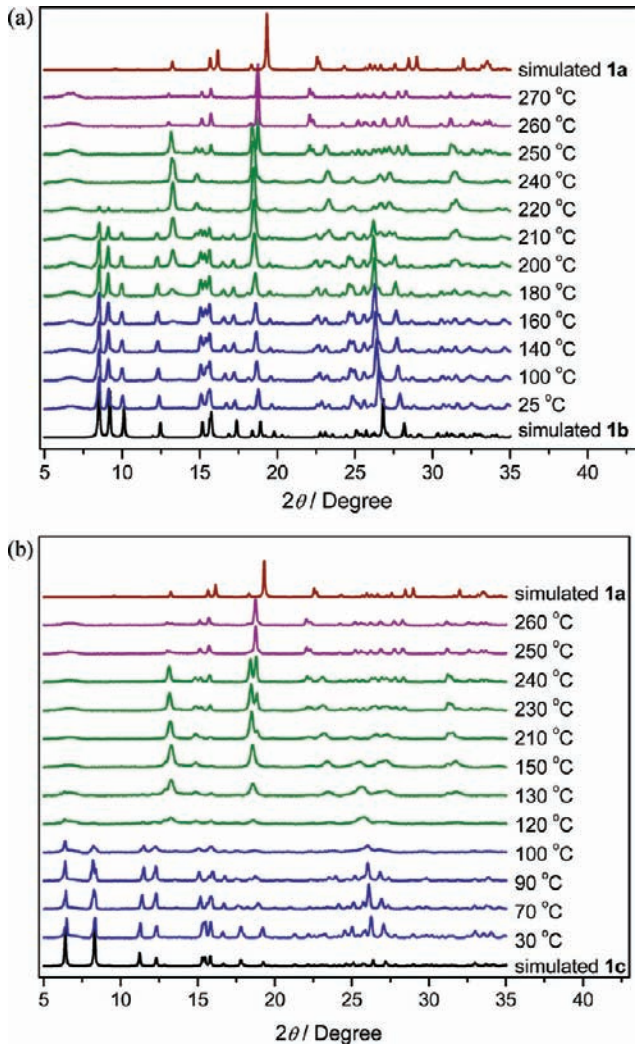

Figure 8. VTPXRD patterns of (a) **1b** and (b) **1c**.

dx.doi.org/10.1021/ic300083k | *Inorg. Chem.* 2012, 51, 4772−4778

thermally stable, nonporous zigzag chain structure, which was confirmed by Rietveld refinement of the PXRD pattern (Table S9 and Figures S3 and S4, Supporting Information). The Ag(I) 2-methylimidazolate isomers **2b**, **2c**, and **2d** also show similar two-step phase transitions. The original structures are stable below 130 °C. The intermediate phase appeared above 140 °C, and the final stable phase (**2a**) appeared above 190 °C (for **2b**, **2c**) and 160 °C (for **2d**), respectively (Figure S5, Supporting Information). Differential scanning calorimetry (DSC) was used to reveal the phase transitions for guest-free **2d** (to avoid the energetic effect of guest removal). The DSC curve of **2d** exhibits a sharp exothermic peak (−43.92 kJ g^{-1}) centered at 153 °C, followed by another broad exothermic one (−20 kJ g^{-1}) centered at 182 °C (Figure S6, Supporting Information), corresponding well to the two-step phase transition. We cannot solve the crystal structures for the intermediate phases, because they always admix with **1b**/**1c** and **1a** or **2b**/**2c**/**2d** and **2a**. The structural transformations from the porous isomers to the nonporous ones for **1** and **2** may be explained by a local melting mechanism, as there is no obvious structural relationship among the superstructures (e.g., packing, position, and short contacts of rings and chains) of these isomers, except the local coordination modes and 0D/1D topologies.

Recently, we reported that Ag(I) 2-isopropylimidazolate [Ag(ipim)] could undergo a similar temperature-induced two-step crystal-to-crystal structural transformation from a chicken-wire isomer to a quintuple helix one.[14] In contrast with **1** and **2**, the stable phase of [Ag(ipim)] at high temperature is not the simple chain (although the simple chain isomer can be synthesized), and there are very similar structural features between the chicken-wire and quintuple helix isomers in favor of a topochemical transformation mechanism. Moreover, there is no observable intermediate phase in the PXRD pattern, and there are a pair of DSC peaks, an endothermic one followed by an exothermic one, during the phase transition.

Sample Activation. According to the structural analysis, except **1b**, other guest-containing isomers might be activated to serve as porous materials. However, from the TG and PXRD results, only **2d** could easily lose the guest molecules and remain in the open structure. When the guest molecules are removed, other isomers undergo phase transitions and very likely transform to nonporous structures. To investigate whether these isomers can be activated at lower temperatures to avoid phase transitions, we performed vacuum thermal desorption (VTD) experiments by recording the guest desorption rate of samples with slow elevation of temperature under high vacuum. The VTD experiment has the same physical meaning as the differential TG curves (DTG) but provides information under high vacuum rather than ambient pressure.

For **1b**, the DTG and VTD curves show sharp peaks at the same temperature (Figure 9a), meaning that the reducing pressure cannot induce an observable effect on the desorption temperature. This fact indicates that the benzene molecules are held very tightly in the crystal of **1b**, because the cavities are isolated. For **1c**, the peak in the VTD curve appears at a temperature 50 °C lower than that in the DTG curve (Figure 9b). Therefore, **1c** could be activated by heating at 80 °C under high vacuum (the same as VTD experiment) for 24 h. TG and PXRD measurements showed that the guest molecules have been completely removed, and the activated sample retains the as-synthesized structure, though the diffraction peaks are weakened and broadened (Figure S7, Supporting Information).

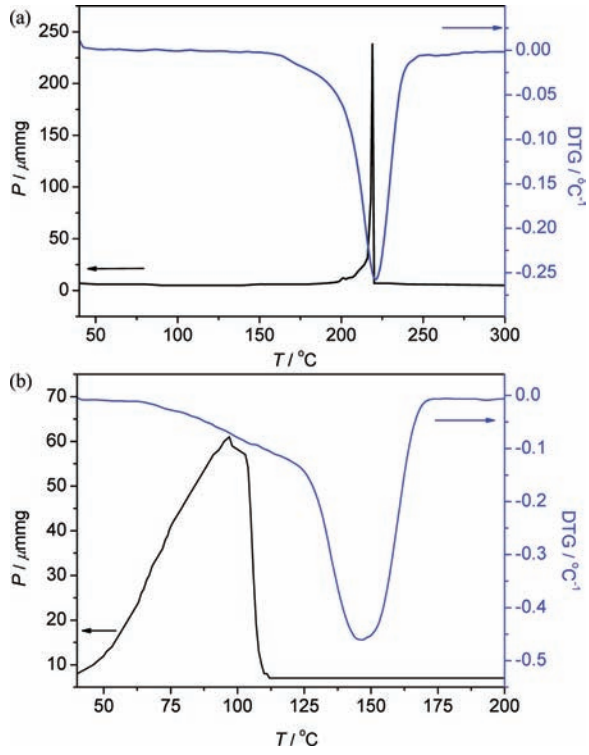

Figure 9. Comparison of DTG and VTD curves of (a) **1b** and (b) **1c**.

Similarly, VTD curves showed that **2b** and **2c** can be readily activated at 60 °C under high vacuum for 24 h, which are also confirmed by TG and PXRD measurements of the activated samples (Figures S8−S10, Supporting Information).

Sorption Properties. In order to confirm the permanent porosity of **1c**, **2b**, **2c**, and **2d**, CO_2 sorption isotherms were measured at 195 K. As shown in Figure 10, all isotherms have

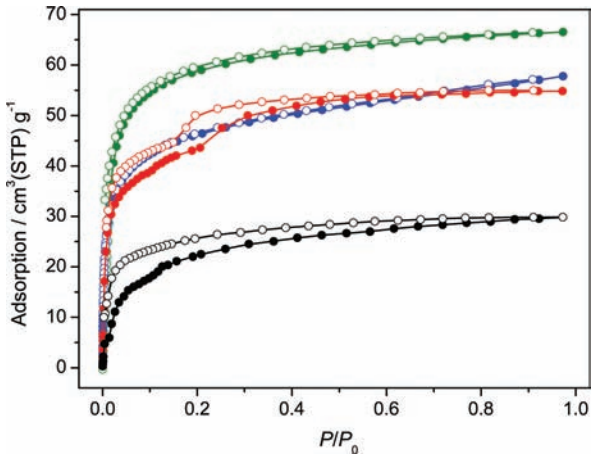

Figure 10. Adsorption (filled) and desorption (open) isotherms of CO_2 for **1c** (black), **2b** (red), **2c** (blue), and **2d** (green) measured at 195 K, respectively.

type-I characteristics, except the small steps and hystereses for **1c** and **2b**, which indicate certain framework flexibility. Fitting the CO_2 adsorption isotherms give large BET (Brunauer−Emmett−Teller) surface areas of 114−286 m^2 g^{-1} and Langmuir surface areas of 181−388 m^2 g^{-1} (Table S10, Supporting Information), indicating that the sorption occurs inside the crystals. The pore volumes of the samples were also

dx.doi.org/10.1021/ic300083k | Inorg. Chem. 2012, 51, 4772−4778

calculated from the saturated uptakes for judging the sample quality. The measured pore volume of **1c** was much less than the theoretical one, indicating partial collapse of the porous framework after guest removal. In contrast, the measured pore volumes of **2b**, **2c**, and **2d** were close to the theoretical ones, confirming that the porous structures were well retained.

CONCLUSIONS

Depending on the chemical nature of targeted coordination polymers and involved metal ions, an appropriate synthetic method and condition should be used. To avoid auto-oxidation of Cu(I) in opened reaction systems, hydrothermal reaction is facile for the syntheses of [Cu(mim)] isomers. On the other hand, to avoid reduction of Ag(I) under hydrothermal conditions and long crystallization period, low purity, and low yield with the liquid diffusion method, the rapid solution mixing method represents an efficient method for the syntheses of [Ag(mim)] isomers. By extensive testing of different reaction solvents and templates with the rapid solution mixing method, the hypothetic octagon isomer of Ag(I) 2-methylimidazolate was successfully synthesized. While a variety of chain and polygon isomers have been known, a rare polyrotaxane-like isomer was found for Cu(I) 2-methylimidazolate, which illustrates the spatial matching of chains and polygons in the aspect of crystal packing.

On the basis of a series of closely related isomers, we were able to study the relationship among pore structure, guest removal, structural transformation, and adsorption property. For example, the Cu(I) octagon, Cu(I) decagon, and Ag(I) octagon, consisting of a different type and number of metal ions, show distinct packing fashions and guest removal behaviors. Interestingly, both the Cu(I) and Ag(I) 2-methylimidazolates undergo similar two-step, crystal-to-crystal structural transformation processes, which have been rarely observed for coordination polymers and may provide insightful information for studying the thermodynamic and dynamic nature of similar materials. Finally, we showed that the vacuum thermal desorption behavior is very useful for determining the activation condition of thermally sensitive open frameworks, as demonstrated by realization of the permanent porosity for the 0D and 1D isomers.

ASSOCIATED CONTENT

Supporting Information

PXRD patterns, TG curves, DSC curves, additional structural plots, DFT calculation data, and X-ray crystallographic files in CIF format. This material is available free of charge via the Internet at http://pubs.acs.org.

AUTHOR INFORMATION

Corresponding Author

*E-mail: zhangjp7@mail.sysu.edu.cn.

Notes

The authors declare no competing financial interest.

ACKNOWLEDGMENTS

This work was supported by the "973 Project" (2012CB821706), NSFC (21121061 and 21001120), and Chinese Ministry of Education (NCET-10-0863 and ROCS).

REFERENCES

(1) (a) Janiak, C. *Dalton Trans.* **2003**, 2781. (b) Chen, B. L.; Xiang, S. C.; Qian, G. D. *Acc. Chem. Res.* **2010**, *43*, 1115. (c) Leong, W. L.; Vittal, J. J. *Chem. Rev.* **2011**, *111*, 688. (d) Uemura, T.; Yanai, N.; Watanabe, S.; Tanaka, H.; Numaguchi, R.; Miyahara, M. T.; Ohta, Y.; Nagaoka, M.; Kitagawa, S. *Nat. Commun.* **2010**, *1*, 83. (e) Xiang, S. C.; Zhang, Z. J.; Zhao, C. G.; Hong, K. L.; Zhao, X. B.; Ding, D. R.; Xie, M. H.; Wu, C. D.; Das, M. C.; Gill, R.; Thomas, K. M.; Chen, B. L. *Nat. Commun.* **2011**, *2*, 204. (f) Takashima, Y.; Martinez, V. M.; Furukawa, S.; Kondo, M.; Shimomura, S.; Uehara, H.; Nakahama, M.; Sugimoto, K.; Kitagawa, S. *Nat. Commun.* **2011**, *2*, 168. (g) Colombo, V.; Galli, S.; Choi, H. J.; Han, G. D.; Maspero, A.; Palmisano, G.; Masciocchi, N.; Long, J. R. *Chem. Sci.* **2011**, *2*, 1311.

(2) (a) Seeber, G.; Cooper, G. J. T.; Newton, G. N.; Rosnes, M. H.; Long, D. L.; Kariuki, B. M.; Kogerler, P.; Cronin, L. *Chem. Sci.* **2010**, *1*, 62. (b) Alkordi, M. H.; Belof, J. L.; Rivera, E.; Wojtas, L.; Eddaoudi, M. *Chem. Sci.* **2011**, *2*, 1695.

(3) Moulton, B.; Zaworotko, M. J. *Chem. Rev.* **2001**, *101*, 1629.

(4) (a) Zhang, J. J.; Wojtas, L.; Larsen, R. W.; Eddaoudi, M.; Zaworotko, M. J. *J. Am. Chem. Soc.* **2009**, *131*, 17040. (b) Yuan, G. Z.; Zhu, C. F.; Liu, Y.; Xuan, W. M.; Cui, Y. *J. Am. Chem. Soc.* **2009**, *131*, 10452. (c) Wang, S. A.; Zang, H. Y.; Sun, C. Y.; Xu, G. J.; Wang, X. L.; Shao, K. Z.; Lan, Y. Q.; Su, Z. M. *CrystEngComm* **2010**, *12*, 3458. (d) Peng, R.; Li, M. A.; Deng, S. R.; Li, Z. Y.; Li, D. *CrystEngComm* **2010**, *12*, 3670. (e) Wang, S. N.; Peng, Y. Q.; Wei, X. L.; Zhang, Q. F.; Wang, D. Q.; Dou, J. M.; Li, D. C.; Bai, J. F. *CrystEngComm* **2011**, *13*, 5313. (f) Cui, P. P.; Wu, J. L.; Zhao, X. L.; Sun, D.; Zhang, L. L.; Guo, J.; Sun, D. F. *Cryst. Growth Des.* **2011**, *11*, 5182. (g) Hu, T. L.; Tao, Y.; Chang, Z.; Bu, X. H. *Inorg. Chem.* **2011**, *50*, 10994. (h) Li, C. P.; Wu, J. M.; Du, M. *Inorg. Chem.* **2011**, *50*, 9284. (i) Weng, D. F.; Wang, B. W.; Wang, Z. M.; Gao, S. *CrystEngComm* **2011**, *13*, 4683. (j) Yang, J.; Ma, J. F.; Batten, S. R.; Ng, S. W.; Liu, Y. Y. *CrystEngComm* **2011**, *13*, 5296. (k) Zhan, S. Z.; Li, M.; Zhou, X. P.; Li, D.; Ng, S. W. *RSC Adv.* **2011**, *1*, 1457. (l) Zhang, B.; Zhu, D. B.; Zhang, Y. *Chem.-Asian J.* **2011**, *6*, 1367.

(5) (a) Zhang, J.-P.; Huang, X.-C.; Chen, X.-M. *Chem. Soc. Rev.* **2009**, *38*, 2385. (b) Makal, T. A.; Yakovenko, A. A.; Zhou, H. C. *J. Phys. Chem. Lett.* **2011**, *2*, 1682.

(6) (a) Wang, X. S.; Ma, S. Q.; Forster, P. M.; Yuan, D. Q.; Eckert, J.; Lopez, J. J.; Murphy, B. J.; Parise, J. B.; Zhou, H. C. *Angew. Chem., Int. Ed.* **2008**, *47*, 7263. (b) Sun, D. F.; Ma, S. Q.; Simmons, J. M.; Li, J. R.; Yuan, D. Q.; Zhou, H. C. *Chem. Commun.* **2010**, *46*, 1329. (c) Chen, S. S.; Chen, M.; Takamizawa, S.; Wang, P.; Lv, G. C.; Sun, W. Y. *Chem. Commun.* **2011**, *47*, 4902.

(7) (a) Zhang, J.-P.; Chen, X.-M. *Chem. Commun.* **2006**, 1689. (b) Zhang, J.-P.; Zhang, Y.-B.; Lin, J.-B.; Chen, X.-M. *Chem. Rev.* **2012**, *112*, 1001.

(8) (a) Huang, X. C.; Zhang, J. P.; Chen, X. M. *J. Am. Chem. Soc.* **2004**, *126*, 13218. (b) Huang, X. C.; Li, D.; Chen, X. M. *CrystEngComm* **2006**, *8*, 351.

(9) Hu, S.; He, K. H.; Zeng, M. H.; Zou, H. H.; Jiang, Y. M. *Inorg. Chem.* **2008**, *47*, 5218.

(10) Perdew, J. P.; Burke, K.; Ernzerhof, M. *Phys. Rev. Lett.* **1996**, *77*, 3865.

(11) (a) Zhang, J. P.; Kitagawa, S. *J. Am. Chem. Soc.* **2008**, *130*, 907. (b) Zhang, J.-P.; Zhu, A.-X.; Lin, R.-B.; Qi, X.-L.; Chen, X.-M. *Adv. Mater.* **2011**, *23*, 1268.

(12) Spek, A. L. *J. Appl. Crystallogr.* **2003**, *36*, 7.

(13) Masciocchi, N.; Ardizzoia, G. A.; LaMonica, G.; Maspero, A.; Sironi, A. *Angew. Chem., Int. Ed.* **1998**, *37*, 3366.

(14) Zhang, J. P.; Qi, X. L.; He, C. T.; Wang, Y.; Chen, X. M. *Chem. Commun.* **2011**, *47*, 4156.